RSC Advances

ROYAL SOCIETY OF CHEMISTRY

www.rsc.org/advances

Journal Name

RSCPublishing

ARTICLE

Sustainable Synthesis of Hollow Cu-loaded Poly(*m*-phenylenediamine) particles and Their Application for Arsenic Removal

Cite this: DOI: 10.1039/xoxxoooooox

Received ooth January 2012,
Accepted ooth January 2012

DOI: 10.1039/xoxxoooooox

www.rsc.org/

Shuo Dai, [a] Bing Peng [a, b] Liyuan Zhang, [a] Liyuan Chai, [a, b] Ting Wang, [a] Yun Meng, [a] Xiaorui Li, [a] Haiying Wang,* [a, b] Jian Luo[c]

A new Cu-catalyzed air oxidation method was successfully developed to prepare Cu-loaded poly(*m*-phenylenediamine) (PmPD) with the monomers conversion rates close to 100%. The polymerization process was examined by the in-situ tracking of open-circuit potential (OCP) and pH. The product was characterized with Scanning electron microscopy (SEM), Transmission electron microscopy (TEM), Fourier transform infrared spectroscopy (FTIR), X-ray photoelectron spectroscopy (XPS), X-ray diffraction (XRD). The result shows Cu catalytic effect in the air oxidation was highly responsible for the great enhancement of monomers conversion rates. As increasing Cu addition, PmPD particles tended to form hollow microstructures, which may be resulted from dehydration effect. Furthermore, the as-obtained samples have superior arsenic(V) removal performance in aqueous solution. The adsorption equilibrium can be rapidly reached within 10 min. Higher Cu-loaded particles exhibited an improved arsenic(V) removal capability of 27.4 mg g^{-1}, much higher than other reports. The adsorption behavior can be well described by Freundlich and pseudo-second-order model. The related possible mechanisms have been explored carefully.

Introduction

As a diamine derivative of polyaniline, poly(phenylenediamine) have many important applications in sensors, catalysis, electrodes and actuators, *etc.*.[1-8] In particular, widespread attention has been attracted on the adsorption performance of Poly(phenylenediamine) over the recent decade due to its superior redox reversibility and chelation ability,[9-12] which can be used for removing various metals ions from water, such as Cr(VI),[13] Hg(II) [14] and Ag(I)[15] . Among the three isomers of poly(phenylenediamine)s, poly(*m*-phenylenediamine) (PmPD) as an adsorbent possesses some important virtues: *i*) insoluble in common solvent, *ii*) high water permeability, *iii*) high production yield, *vi*) synthesis without high temperature or acid solvents. Many developments of poly(*m*-phenylenediamine) have been made by Li and our groups, in terms of molecular structures,[16] monomer conversion efficiency[17] and morphology.[15] The improved nanoscaled particles exhibits superior adsorption capability of Ag(I) (2359.3 mg g^{-1})[15] and Orange G (387.6mg g^{-1}).[17]

Generally, the conventional chemically oxidative polymerization is the most accepted method for synthesizing polyaniline and its derivatives, due to its mass production and simple processes. However, introducing a large amounts of costly oxidants (e.g. persulfate) is the prerequisite to initiate the polymerization, which definitely give rise to concentrated salt water (e.g., Na_2SO_4)[18] with plenty of unreacted monomers or even toxic oligomers dissolved in bulk solution after polymerization.[19, 20] To prevent the mass production of sulfates, adopting green oxidants is another effective strategy, such as H_2O_2 or O_2. Nevertheless, the synthesis yields in previous reports remained quite low (generally not exceeding 40%), which meant more abundant toxic organic chemicals left in the bulk system.[21-23] To date, it is still a challenge problem to improve polymerization efficiency of mPD.

In this context, it is reasonable to conclude that a sustainable synthesis of conjugated polymers, including the poly(*m*-phenylenediamine), must involve two indispensable elements: *i*) side-products from oxidant decomposition should be totally harmless and *ii*) ultrahigh conversion rate that leaves nearly no toxic organic chemicals in polymerization solution. Unfortunately, seldom synthesis has fulfilled these two requirements.

In present research, we developed a sustainable synthesis of poly(*m*-phenylenediamine) microparticles with hollow structures via Cu-catalyzed air oxidation. The conversion efficiency of monomer in this research can reach close to 100%, which is higher than the highest yield reported (93.1%)[24]. More profoundly, the nanoscaled Cu-loaded PmPD particle is a hopeful material in arsenic removal in aqueous solution. This study is the first to present detailed investigations of As(V) removal performance and mechanisms by Cu-loaded PmPD particles.

Experimental

Materials

The chemicals were of analytical grade. $CuCl_2 \cdot 2H_2O$ and $Na_3AsO_4 \cdot 12H_2O$ were purchased from Sinopharm Chemical (Shanghai, China), while the *m*-phenylenediamine (mPD) was from Acros (Belgium). Organic solvents, such as ethanol (EtOH), dimethylformamide (DMF), N-methyl-2-pyrrolidone (NMP) and Dimethyl sulfoxide (DMSO) were from Hui-Hong Chemical (Hunan, China).

Preparation of Poly(*m*-phenylenediamine) particles

Typical synthetic processes of poly(*m*-phenylenediamine) (PmPD) hollow sub-microparticles were as follows: 3.0 g mPD (monomer) was dissolved into 100 mL aqueous solution to form the monomer solution in 250 mL single-neck flat bottom flask. The monomer solution was pre-warmed to 30 °C and kept stirring by an IKA RCT basic magnetic stirrer at a speed of 1000 r s^{-1}. Then 10 mL of solution with a specific concentration of Cu^{2+} (its temperature was also 30 °C) was added to the monomer solution in one pot. And air was introduced into the mixture as soon as the addition of Cu^{2+} solution. And air velocity was 40 L min^{-1} by air pump and rubber hose was used to connect reaction system with air pump (ESI-1). Then, the reaction system was kept on stirring with air for 24 hours. The equipment and synthesis sketch map is illustrated in ESI-2. The resulting mixture was separated by filtration and rinsed with to remove the impurity by using sand cored funnel (G5) which pore size was about 1.5~2.5μm. During filtration, used 50 mL distilled water to wash the reaction vessel and 50 mL to rinse PmPD particles, and then took this 100 mL filtrate and the initial filtrate of 100 mL, a total of 200 ml, to measure total organic carbon (TOC) and Cu mass. The product was dried at 60 °C in air for more than 12 h. The PmPD particles was named as PmPD-Cu*x* (*x*: 1:1, 1:0.5, 1:0.25, 1:0.125 and 1:0.1), where *x* corresponds to the mPD: Cu^{2+} molar ratio and *y* corresponds to the reaction time (h), respectively. And then, the conversion rate *Y* (%) of monomers in polymerization can be calculated according to the following equation:

$$Y = (1 - \frac{c \times V \times M_{mPD}}{6M_c \times m_0}) \times 100\% \quad (1)$$

where *c* (g L^{-1}) and *V* (L) are the concentration of TOC and the volume of the filtrate, M_{mPD} (g mol^{-1}) and M_c (g mol^{-1}) are the molar mass of mPD (108 g mol^{-1}) and carbon (12 g mol^{-1}), and m_0 (g) is the dosage of the initial mPD.

Characterization

Fourier transform infrared spectroscopy (FTIR) of products was collected via Nicolet IS10 infrared spectrometer in the range of 4000-1000 cm^{-1} with resolution of 4 cm^{-1}. Raman (LABRAM-HR 800, 514 nm He-Ne laser excitation) were applied to study the molecular structure of PmPD. The Atomic Absorption spectrometry (WFX-200 AAS) was applied to test the Cu content in the filtrate. Before detection, the PmPD particles or solution was digested by a mixed solution of HCl and HNO_3.[25] JSM-6360 scanning electron microscopy (SEM) and TECNAI G2 transmission electron microscopy (TEM) were used to get the morphologies of the PmPD particles, with accelerating voltages of 20 kV and 120 kV, respectively. The X-ray diffraction (XRD) pattern was collected on a D/Max 2500 VB+X X-ray diffractometer using Cu (40 kV, 300 mA) radiation. X-ray photoelectron spectroscopy (XPS) measurements were carried out on a Thermo Fisher Scientific K-Alpha 1063 using Al Kα X-ray as the excitation source. The Inductively Coupled Plasma Atomic Emission Spectrometry (ICP-AES, Intrepid II XSP Radial) was used to detect the arsenic in the solution after adsorption. TOC was measured by TOC-VCPH.

The solubility of products was investigated semiquantitatively as follows: 10 mg of PmPD particles was added into 10 mL of the solvent and the solution was shaken for 24 h at room temperature. After filtration, the filtrate was collected for calculation.[26]

Adsorption experiment

In the batch experiments, 20 mg of PmPD particles was added into 40 mL of As(V) aqueous solution with pH 5 ± 0.2 at 35 ºC and shaken for a specific time (0-12 h). The solution pH was adjusted with HCl and NaOH solution. After filtration, the arsenic concentration in the filtrate was measured by ICP-AES.

The adsorption isotherm was obtained by varying the initial arsenic concentrations and stirring for 12 h (concentration range: 0-80 mg L^{-1} for As(V)). The equilibrium adsorption capacity (q_e) (mg g^{-1}) for arsenic was calculated according to the following equation (2). The Langmuir (3) and Freundlich (4) models were used to study the isotherm adsorption behavior of the PmPD particles.

$$q_e = \frac{c_0 - c_1}{m} \times V_1 \quad (2)$$

$$\frac{c_e}{q_e} = \frac{c_e}{q_m} + \frac{1}{K_a q_m} \quad (3)$$

$$\log q_e = \frac{1}{n} \log c_e + \log K_f \quad (4)$$

where c_0 and c_1 (mg L^{-1}) are the arsenic concentration of the solution before and after adsorption, *m* (mg) is the dosage of the PmPD particles and V_1 (mL) is the volume of arsenic solution. q_m (mg g^{-1}) is the maximum adsorption capacity, c_e (mg L^{-1}) is the equilibrium concentration of arsenic in the filtrate, K_a (L mg^{-1}) is the adsorption coefficient, K_f and *n* are the equilibrium and constants, respectively.

The adsorption kinetics was investigated with the initial As(V) concentration of 3.7 mg L^{-1} at pH of 5.0 and adsorbents dose of 0.5 g L^{-1}. The solution was allowed to shake with the adsorbent at 35 °C for a special time (10 ~ 720 min).

The pseudo-first (5) and -second (6) order rate equations were used to test the kinetic process of adsorption:

$$\log(q_e - q_t) = \log q_e - \frac{k}{2.303} t \quad (5)$$

$$\frac{t}{q_t} = \frac{1}{h} + \frac{t}{q_e} \quad (6)$$

where q_e (mg g^{-1}) is the equilibrium arsenic adsorbance of the PmPD particles, q_t (mg g^{-1}) is the arsenic adsorbance of the PmPD particles at specific time (t, h), *k* and *h* are the rate constants of first and second order equations, respectively.

The initial pH of the solution was controlled by HCl or NaOH from 3 to 9 for research the effect of pH on adsorption. And Cl^-, SO_4^{2-}, NO_3^-, PO_4^{3-} were investigated as the competing anions and the molar proportion of competing anions to AsO_4^{3-} was controlled from 1:1 to 4:1.

Results and discussion

Efficiency of Cu-catalyzed air oxidation

The polymerization of mPDs in Cu-catalyzed air oxidation system was investigated. As shown in Figure 1, Cu addition has a significant effect on the polymerization efficiency. Without Cu addition, no obvious solid particles could be filtered out after the 24 h polymerization finished, except that the bulk solution became brown. This is quite consistent with the previous reports[21, 22], indicating that the oxidation ability of pure air oxidation system cannot effectively afford the polymerization of mPD. However, when Cu amount increased to n_{mPD}:n_{Cu}=1:0.1, the monomers conversion rates rapidly rise to 49%. Especially, when Cu amount further increased to n_{mPD}:n_{Cu}=1:0.25 and more, the conversion rates continued to grow rapidly and reached close to 100%, this is far more than previous reports stated up to our knowledge (e.g. 93%)[24]. Especially, the obtained filtrates (before distilled water rinsed) appeared to be transparent, clean without any obvious suspended solids. The TOC remaining in the filtrates were below <10 mg L^{-1} (in ESI-3), which is compliant with the discharge standard of the United States Environmental Protection Agency.[27]

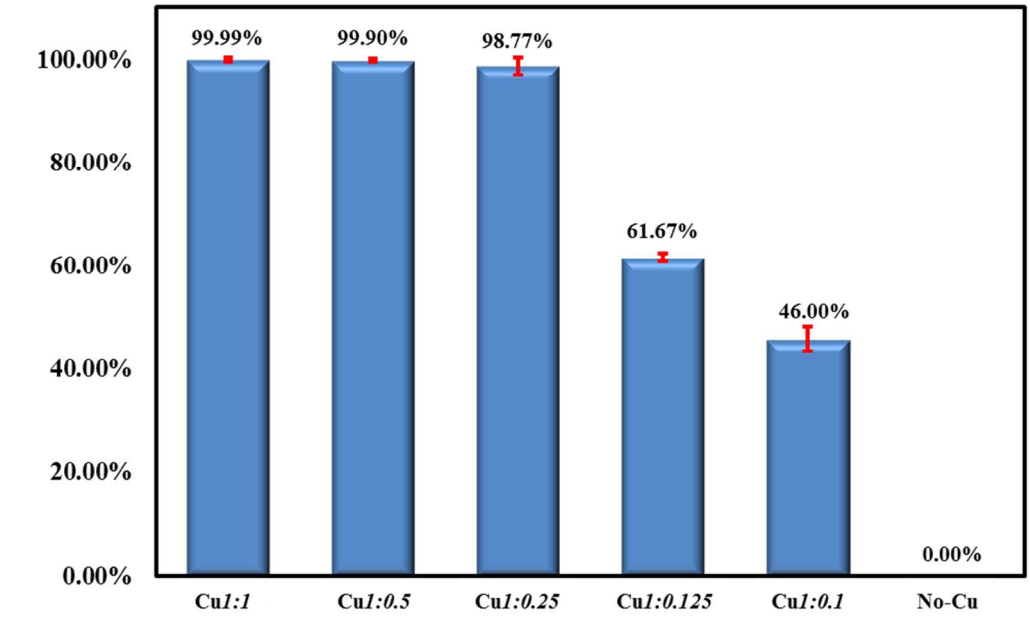

Figure 1 Conversion rate of PmPD-Cu*1:1*, PmPD-Cu*1:0.5*, PmPD-Cu*1:0.25*, Cu*1:0.125*, Cu*1:0.1* and No-Cu.

Of course, large amounts of Cu (65~878 mg) were still remained in the filtrates after polymerization (ESI-3). To test the recyclability of these filtrates including residual Cu (TOC <10 mg L^{-1}, which is within the EPA limits), a comparable experiment was designed by directly adding certain amount of Cu and mPD into the said filtrates to make up nmPD:nCu=1:0.5. The other procedures were the same as the above-mentioned method. Actually, the monomers conversion rate can also reach to 98.97%. That strongly demonstrated that the filtrates can certainly be re-used for the PmPD polymerization (ESI-2) without any other treatments. Effective utilization of the obtained filtrates can greatly improve process cost and substantially prevent secondary pollutions to the maximum during the PmPD synthesis.

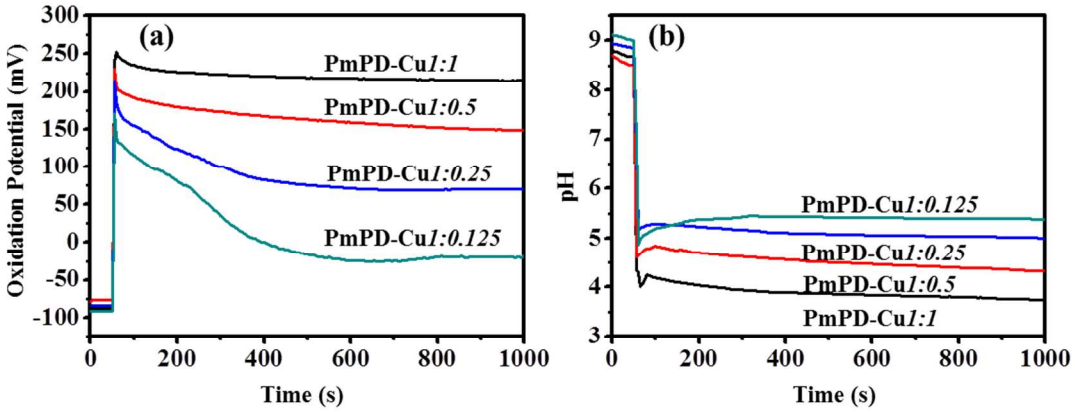

Figure 2 (a) Open-circuit potential and (b) pH of the polymerization.

To explore the polymerization process, open-circuit potential (OCP) and pH of the reaction system were monitored in-situ, as shown in Figure 2. As soon as the Cu^{2+} solution added into monomer solution, the polymerization OCP suddenly rose to more than 150 mV which was ascribed to the oxidizability and coordination of Cu^{2+}[28-30]. The Cu^{2+} could readily react with the monomers to form the complexes and the Cu^{2+} was reduced to the corresponding Cu^{+}, which has been proven by

our previous study [17, 24]. It can explain the OCP dropped sharply after finish adding the Cu^{2+} solution. As reflected by the color, the polymerization system rapidly changed from clean transparent to dark brown with lots of solids suspended. From Figure 2 a, the higher solution potentials apparently can be obtained with the increased Cu:mPD ratios after air introducing. Moreover, the increased Cu amounts also decreased the final solution pH (Figure 2 b) which was resulted from H^+ release from mPD during the oxidation. It clearly demonstrates that the air oxidation was activated significantly through employing Cu^{2+}. Especially, the solution potential with air introducing gradually declined to a relatively constant value. That is to say, the oxidation reaction remains steady in the solution. However, the exact mechanism is still unclear, yet it is apparently a consequence of catalytic air oxidation via Cu coordination with monomers. During the polymerization, the reduction of Cu^{2+} to Cu^+ triggered the oxidation of monomer and polymerization, while the O_2 in air could easily oxidize the Cu^+ to Cu^{2+} again.[22] This reversible process promised a dynamic balance for the oxidation.

Taken together, the presented Cu-catalyzed air oxidation provides a significant strategy for the sustainable and high efficient synthesis of PmPD particles.

Morphology of PmPD particles

The morphology of PmPD particles was measured by the SEM and TEM (Figure 3 and ESI-4). Obviously, amount of Cu addition have a significant influence on the micro-morphology of PmPD particles. As shown in Figure 3 (g, h), the product synthesized in n_{mPD}:n_{Cu}=1:0.125 just consisted of abundant irregular solid particles. However, great variation emerged by increasing Cu content. When mPD/Cu ratio became 1:0.5, a lot of distinguishable solid microspheres appeared actually in the product, though their surfaces are very rough (Figure 3 c, d). It is noted that some hollow nanostructures could be identified apparently in Fig 3 (d). Especially, in a further experiment, the obtained PmPD-Cu*1:1* particles were mainly composed of nanosized smooth spheres with the diameters of 300~500 nm (Figure 3 a, b). More importantly, the microspheres are hollow with a wall thickness of about 60-80 nm, as confirmed by the TEM image. Up to our knowledge, that is a new sustainable alternate to constitute hollow structure of PmPD particles.

To give insight to these morphologies variations, some samples were separated from the reaction solution with mPD/Cu ratio of 1:1 before air introduction and after reaction for 6h, and then characterized using TEM. On account of the reaction of the Cu and monomer was very strong and fast. When Cu^{2+} solution was added, the color of solution suddenly turns to black from transparent and particulate matter could be found immediately. ESI-4a was obtained by separate the solution in this time; primarily consisted of hollow nanorods with the length of 400~500 nm, the diameters of ~100 nm and wall thickness of 20~30 nm. When the reaction time reached 6 h, the aggregates greatly changed into nanosized spheres with the increased diameters of 200~400 nm and wall thickness of 60~80 nm (in ESI-4b), just similar to the final product (Figure 3 a, b). More importantly, a fission phenomenon among these aggregates was evidently observed (in ESI-4b), which showed a tendency to split the nanorods into the nanospheres. It strongly demonstrated that the initial micromorphology of the synthesized particles definitely possessed the hollow rod-like nanomorphology, which finally was changed into the hollow nanospheres.

The self-formation mechanism of the hollow structures can be described as follows. When in contact with Cu^{2+}, mPD instantly reacted to generate the positively charged complex, which would increase the molecules amphiphilicity to constitute micelles in water. As higher amount of Cu(II) salt was added into the system, the counter ion concentration also

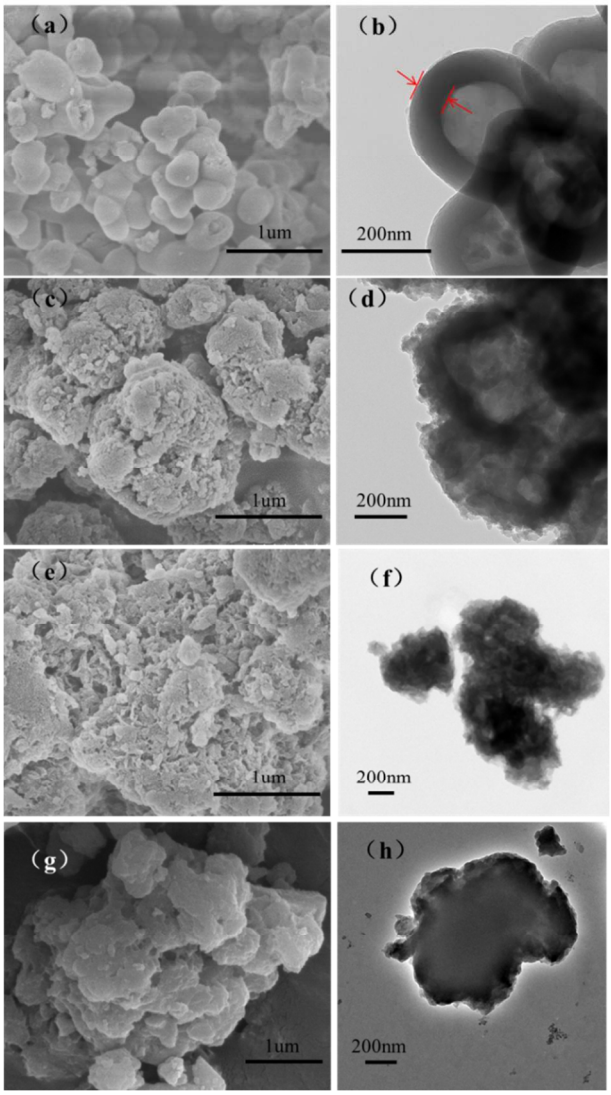

Figure 3 SEM and TEM images: (a, b) PmPD-Cu*1:1*; (c, d) PmPD-Cu*1:0.5*; (e, f) PmPD-Cu*1:0.25* and (g, h) PmPD-Cu*1:0.125*. (Reaction time was 24 hours).

increased, which can compress the electrical double layer and reduce charge repulsion, allowing the micelles to come closer to each other[31-33]. At the same time, the increased ionic strength can cause the molecules' polar groups undergo more ''dehydration'' to enhance their hydrophobic character, which will greatly reduce monomers exchange between the micelles and the bulk phase.[34] Hence, the effects worked together to drive micellar molecules to be rearranged to form enlarged stable micellar cluster or bilayer aggregates, just like the obtained nanorods as ESI-4.[34] When air was introduced into the bulk solution, the oxidation chain-propagation will principally takes place around the surface of the aggregates to make them growing up.[32] However, when the reaction reached to a certain extent, the dynamic equilibrium cannot be maintained between the grown aggregates and polymer

molecules. The nanorods will spontaneously split into nanosized spheres by fission. Particularly, if the total Cu addition is not enough, low ionic strength will go against keeping hollow aggregates stable and finally formed irregular solid particles.

Structural characterization

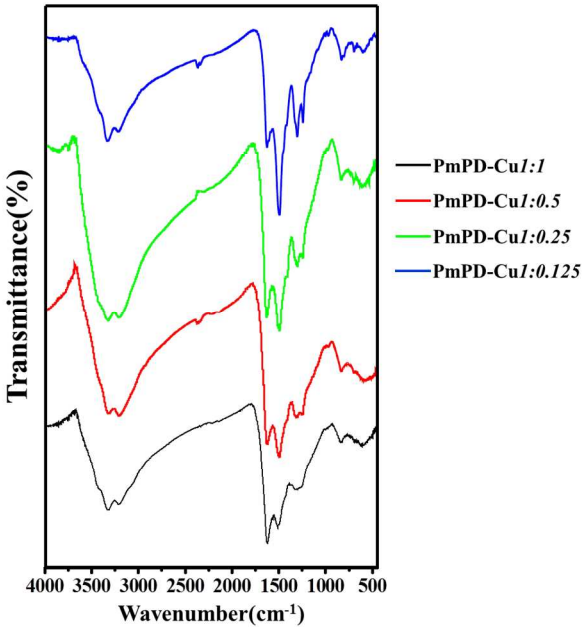

Figure 4 FTIR spectra of PmPD-Cu*1:1*, PmPD-Cu*1:0.5*, PmPD-Cu*1:0.25* and PmPD-Cu*1:0.125*.

The molecular structures of PmPD-Cu*x* (*x*: 1:1, 1:0.5, 1:0.25, 1:0.125, 1:0.1) were investigated by FTIR (Figure 4). As seen in Figure 4, the FTIR spectra of these four polymers were similar. The broad absorption centered between 3500 and 3000 cm^{-1} should be due to the stretching mode of -NH-.[35-37] The peak at ~1620 cm^{-1} was associated with phenazine and quinoid imine. And the peak at ~1500 cm^{-1} was attributed to benzenoid amine structures.[38-40] Meanwhile, the peak at ~1250 cm^{-1} corresponded to the C-N stretching mode in the PmPD.[41] Moreover, it was found that the relative content of the two peaks changed obviously with the variation of the Cu/monomer molar ratio. With the increase of Cu^{2+}, the peak at ~1620 cm^{-1} turned to stronger which indicated that content of phenazine and quinoid structure were increased. Generally speaking, Cu/monomer molar ratio was an effective factor on the variations of oxidation state.

Except for FTIR, Raman spectra were also used to analyses the structures of obtained PmPD particles in ESI-5. The peak at ~1573 cm^{-1} was attributed to quinoid. While the two peaks at ~1330 and ~1410 cm^{-1} were attributed to $C{\sim}N^{+}$ and phenazine structure, respectively.[42] It was found that the relative intensity of phenazine increased with the enhancement of Cu^{2+} amount. The increase of phenazine structure should be resulted from the oxidation of linear benzenoid structure.[40] This indirectly verifies the increased oxidation state of PmPD with promoting the Cu:mPD ratio, which was in line with the analysis of FTIR. On the other hand, the $C{\sim}N^{+}$ was caused by the chelation of imine groups by Cu^{2+}.

Instead of FTIR and Raman, the empirical composition, functional groups on the surfaces, chemical state and electronic state of the elements within the PmPD particles were quantitatively determined by XPS technique. Figure 5 was the typical survey spectra from 0 to 1400 eV of the samples. It clearly indicates that the PmPD particles with Cu loaded are basically made up of carbon, oxygen, nitrogen, copper and a small amount of chlorine. With the decrease of the initial dosage of Cu^{2+}, the peak of Cu became weaker.

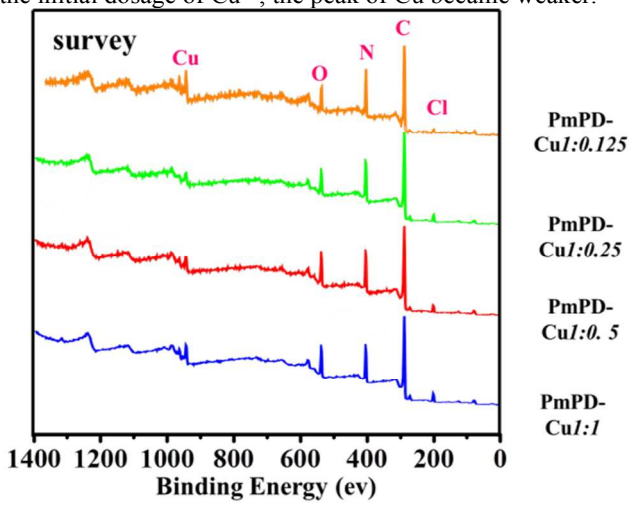

Figure 5 Wide energy range surface spectra of PmPD-Cu*1:1*; PmPD-Cu*1:0.5* PmPD-Cu*1:0.25* and PmPD-Cu*1:0.125*.

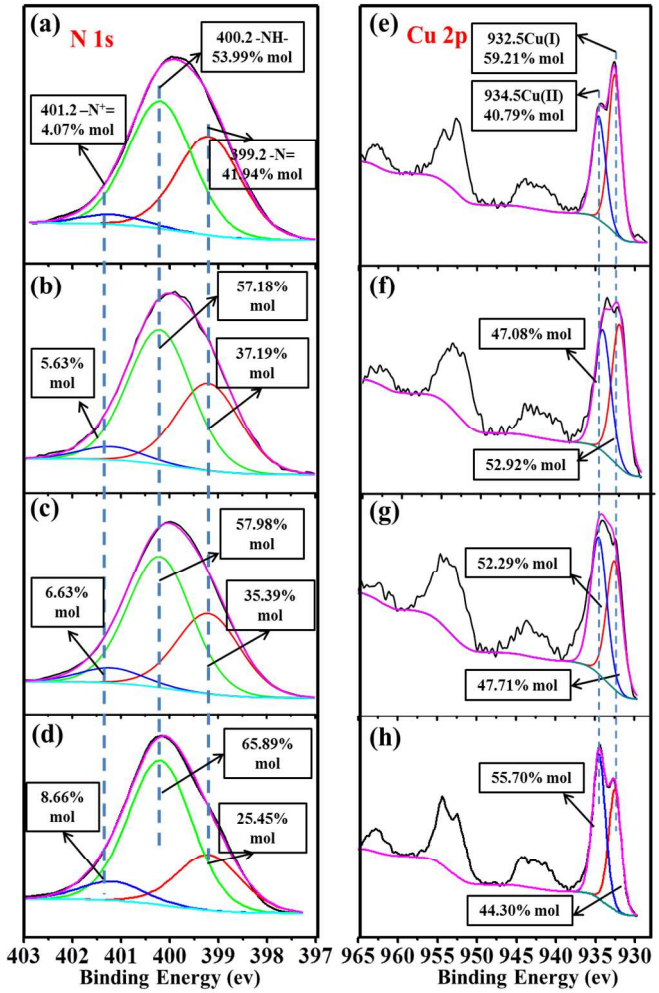

Figure 6 Deconvolution results of N 1s (a-d) and Cu 2p (e-h) XPS spectra of PmPD-Cu*1:1* (a, e), PmPD-Cu*1:0.5* (b, f), PmPD-Cu*1:0.25* (c, g) and PmPD-Cu*1:0.125*.

Here, as shown in Figure 6(a-d), the XPS spectra of N element of various PmPD particles were investigated to study the relative molar contents of N-containing segments. The peak at 399.2 eV was associated with the neutral –N= in both quinoid imine and phenazine while the one at 400.2 eV was due to the –NH– in the benzenoid amine units. Beside these, there was a weak peak at 401.2 eV assigned to $–N^{+}=$.[43-45] With the increase of Cu^{2+}, the area of –N= and $–N^{+}=$ increased, indicating the enhancement of oxidation state. This was in agreement with the analysis of FTIR and Raman. The presence of $–N^{+}=$ prove that Cu^{2+} was chelated on the PmPD, which was in agreement with literatures.[9, 44] Based on XPS analysis, it was interesting to see that the oxidation state of PmPD increased with the increase of Cu/monomer molar ratio. The XPS spectra of Cu element of PmPD particles were also shown in Figure 6(e-h). Obviously, copper existed in two oxidation states on the PmPD particles, Cu^{2+} and Cu^{+}.[46-49] Cu^{+} contents tended to rise with the increase of Cu/mPD ratio. The variation of Cu^{+} contents proved that Cu^{2+} was involved in the mPD oxidation polymerization. It was the reduction of Cu^{2+} to Cu^{+} achieving the oxidation and the increased amount of Cu^{+} was possibly a direct reason for the increased oxidation state of PmPD. Therefore, it could be further correlated to the increase of conversion rate.

The supermolecular structure of PmPD particles was characterized by XRD (Figure 7). As shown in Figure 7, there was one broad peak in these five patterns located at ~25 to 28°, which was a typical characteristic for amorphous structure.[50] Generally speaking, an amorphous structure was conducive to the penetration and then adsorption of ions onto the macromolecules due to the loose and disordered piles of the polymeric chains in the amorphous structure.[9, 26, 50] No peak observed in the range of 14-68°, suggesting that Cu, Cu_2O and CuO did not exist[51, 52] which indicating that Cu^{2+} was chelated to PmPD consistent with XPS analysis.

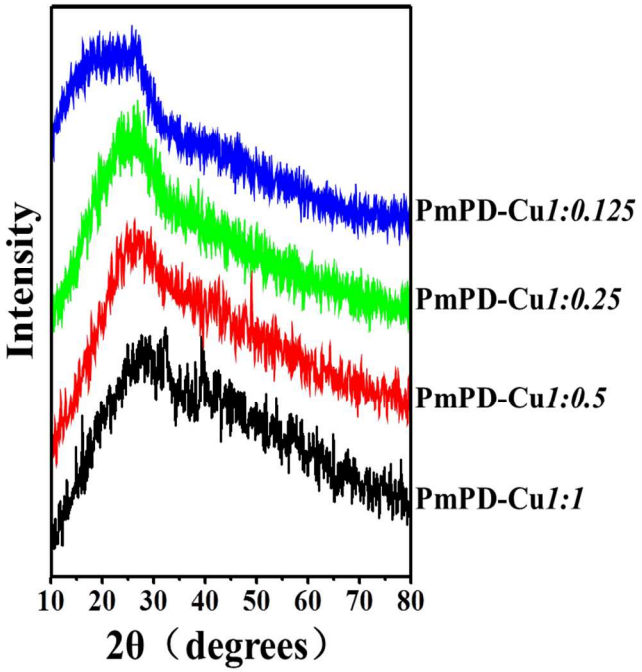

Figure 7 XRD patterns of PmPD-Cu*1:1*, PmPD-Cu*1:0.5*, PmPD-Cu*1:0.25* and PmPD-Cu*1:0.125*.

In addition, the solubility of PmPD particles in H_2O, DMF, EtOH, NMP and DMSO is listed in Table 1. As seen, the solubility of the five PmPD particles in H_2O, DMF, EtOH, NMP and DMSO is very poor. The insoluble or slightly soluble property is suitable as adsorbent.

Table 1 The Solubility of PmPD particles.

PmPD-name	Solubility[a]				
	H_2O	DMF	EtOH	NMP	DMSO
Cu*1*	IS	SS	IS	IS	SS
Cu*0.5*	IS	SS	IS	IS	SS
Cu*0.25*	IS	SS	IS	IS	SS
Cu*0.125*	IS	SS	IS	SS	SS
Cu*0.1*	IS	SS	IS	SS	SS

[a] IS and SS represent the sample is insoluble or slightly soluble in a specific solvent.

Arsenic adsorption ability of PmPD particles

Effect of initial arsenic concentration. Figure 8 shows the As(V) adsorption performance of various PmPD particles under different initial arsenic concentrations (0-80 mg L^{-1}). It should be note that PmPD particles without Cu (PmPD-Cu*0*) was synthesized with persulfate as oxidant based on the previous report[35], which was used to treat the arsenic solution, since no PmPD products can be effectively collected by air oxidation without Cu addition.

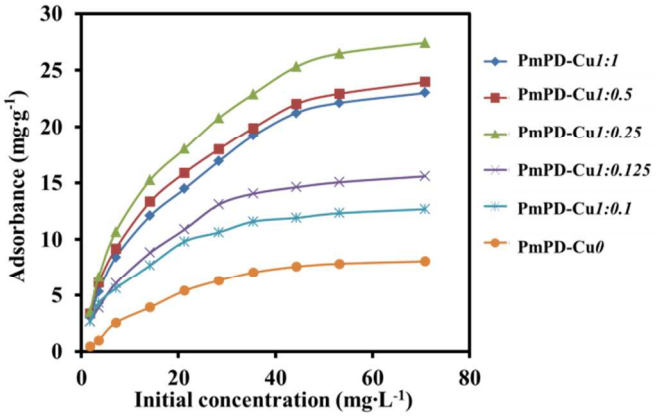

Figure 8 Effects of initial concentration of PmPD particles. (T=35 °C; adsorbent doses=0.5 g L^{-1}; pH=5 ± 0.2)

As shown in Figure 8, when initial As(V) concentration is 70 mg L^{-1}, PmPD-Cu*0* exhibited a certain arsenic adsorbance as low as about 8 mg g^{-1}. As the Cu/mPD ratios rose, the adsorbance of PmPD particles loaded with Cu significantly increased. The maximal adsorbance (about 27.4 mg g^{-1}) occurred at Cu/mPD ratios 0.25:1, 4 times as much as that of PmPD-Cu0. Subsequently, further enhancing Cu/mPD ratio had no great impacts upon the As(V) adsorption of PmPD particles with just a slight decrease to about 23-24 mg g^{-1}.

It is indicative that Cu played a crucial role in the arsenic removal of PmPD particles. Consequently, PmPD-Cu*1:0.25* is more preferable adsorbent for As(V) removal.

To give a deeper analysis on the isotherm adsorption, math models, *e.g.*, Langmuir and Freundlich were used to fit the data above. Results are given in ESI-6. It summarizes the correlation coefficients (R^2) of Langmuir and Freundlich isotherms of PmPD-Cu particles. The Freundlich can better describe the adsorption since the correlation efficiency of

Freundlich is all much higher than that of Langmuir. This suggests that PmPD particles adsorption of arsenic is a multicomponent adsorption isotherm which is derived based on the assumption that an exponential distribution of adsorption energies exists for each component. [53] The maximal capacity reached 27.4 mg g^{-1} for PmPD-Cu*1:0.25*. To demonstrate the advantage of the PmPD with Cu loaded, a comparison between them and some similar kind of reported adsorbents is provided in Table 2. [54-57] It is obvious that the Cu loaded PmPD particles have a superior As removal performance in aqueous solution.

Table 2 Comparison of the adsorption capacity of arsenic on PmPD-Cu particles with reported materials.

Adsorbent sample	pH	Removal capacity for As (V) (mg g^{-1})	Reference
PmPD-Cu*1:1*	5	24.51	this work
PmPD-Cu*1:0.5*	5	24.60	this work
PmPD-Cu*1:0.25*	5	28.13	this work
PmPD-Cu*1:0.125*	5	16.63	this work
PmPD-Cu*1:0.1*	5	13.12	this work
PmPD-Cu*0*	5	11.24	this work
Fe_3O_4 Particles	5	7.23	[54]
Ni/NixB nanoparticles coated resin	6	17.8	[56]
CTS-g-PA	7.2	6.56	[55]
Acidithiobacillus ferrooxidans BY-3	4.0	0.333	[57]

Effect of adsorption time. Figure 9 shows plots of residual arsenic amount in the filtrate versus adsorption time for the PmPD-Cu*1:0.25*. The adsorption process can be roughly divided into fast and slow steps. The fast step lasted for about 10 min; the residue percentage of arsenic in the filtrate was sharply decreased to 18.5% for. This rapid process was caused by the adsorption of arsenic to the functional groups on the surface of PmPD particles. As prolonging the time, the adsorption becomes slow apparently, owing to the gradual diffusion of arsenic molecules from the surface to the inner structures of the PmPD particles. This rapid attainment of adsorption equilibrium is a great important to the practical process of the obtained PmPD particles.

For a further analysis, the pseudo-first-order and -second-order adsorption models were used to fit the above data and results are listed in ESI-7. It summarizes the kinetic parameters and the R^2. As can be seen, the pseudo-second-order kinetic model (>0.99) is better for describing the adsorption process, because of its higher correlation efficiency than the pseudo-first-order kinetic model (<0.97). The initial adsorption rate of arsenic onto the PmPD particles is in the range from 0.74 to 2.38 mg g^{-1} min^{-1}. Noticeably, the establishment of the pseudo-second-order model is based on the fact that the interaction force between adsorbent and adsorbate is chemisorption process.[9] That is to say, arsenic removal of PmPD particles is probably a chemical adsorption process.

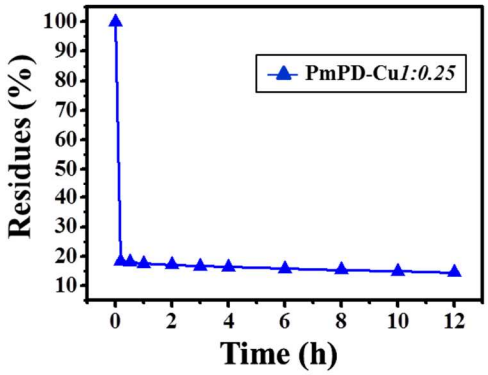

Figure 9 Effects of time on the adsorption performance of PmPD-Cu*1:0.25* particles. (T=35 °C; adsorbent doses=0.5 g L^{-1}; pH=5 ± 0.2)

Effect of initial pH. Arsenic removal property of PmPD-Cu*1:0.25* was measured with initial pH value from 3 to 11 (Figure 11). The removal rate was calculated according to the equations described in the literature.[10] When decreasing the pH from 5.0 to 3.0, the removal rate declines obviously from only 53.2% to 16.1%. This means that the acidic condition with pH lower than 5 is not beneficial for arsenic removal. While at pH 5.0~7.0, the removal rate varies little (<2%), implying that the weak acidic condition influences slightly on arsenic adsorption. As pH from 5 decrease to 3, negative charged $H_2AsO_4^-$ began to turn to neutral molecular state H_3AsO_4, which is difficult to be adsorbed, thus leading to the decrease of removal rate. As pH increased to 11, the removal rate of arsenic rapidly dropped to 0%, which is mainly due to OH^- competition in alkaline condition. As a consequence, the solution pH at 5.0~7.0 is suitable for arsenic adsorption of PmPD particles.

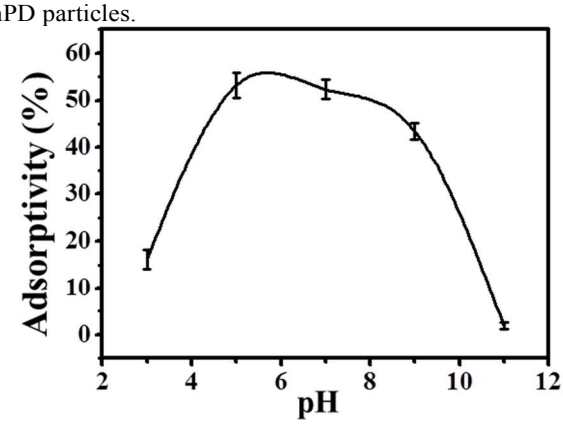

Figure 10 Effect of pH on the adsorption performance of PmPD-Cu*1:0.25* particles. (T=35 °C; adsorbent doses=20 mg L^{-1})

Competitive adsorption. The competitive adsorption ability of PmPD-Cu*1:0.25* in the coexistence of interference anions was studied, such as Cl^-, SO_4^{2-}, NO_3^- and PO_4^{3-} (ESI-8). From

ESI-8, the PmPD particles follows the selectivity pattern $Cl^- > NO_3^- > SO_4^{2-} > PO_4^{3-}$. The influence of Cl^- and NO_3^- on AsO_4^{3-} adsorption is weak and negligible while SO_4^{2-} and PO_4^{3-} have negative effect. It demonstrates the outstanding selectivity of PmPD particles toward AsO_4^{3-} in Cl^- and NO_3^-.

Adsorption Mechanism of As(V) onto PmPD particles. To clarify the adsorption mechanism, PmPD particles before and after arsenic adsorption were characterized by XPS. The As 3d and N 1s data (XPS) of PmPD particles and relevant calculation are given in Figure 11.[9, 58] Based on the As 3d data, the adsorption of As on PmPD particles existed in two forms, 58.14% mol As(V) and 41.86% mol As(III). That means an oxidation process took place to make As(V) reduced to As(III) during the adsorption. As compared the data of N1s before and after adsorption (in Figure 11), it can be found that the content of –NH– declined by 5.7% after treating As(V), in-turn the content of =N– and $=N^+$– increased correspondingly.

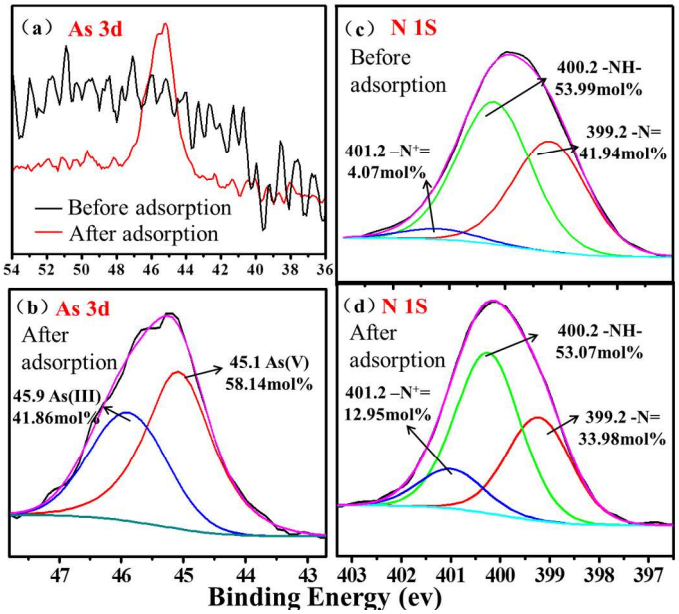

Figure 11 Deconvolution results of N 1s and As 3d XPS spectra of PmPD-Cu*1:1* after adsorption.

As is known to all, –NH– of conjugated polymers can be oxidized readily and then hydrogen left, which was finally transformed to =N–.[44] That is to say, 0.92% of –NH– was oxidized by As(V) form to =N–. On the other hand, the electron density of =N– is much higher than that of –NH– due to its different molecular configuration,[59, 60] which allows it to interact with As(III) cations through coordination. The increased amount of $=N^+$– after adsorption also strongly verifies this chelation between As(III) and =N–. It should be noted that part of the =N– in PmPD before adsorption has been already chelated by Cu ions to generate $=N^+$– which can interact with negative ionic As(V) through static manner. Based on the discussion of XPS, the corresponding interaction was illustrated in Scheme 1.[44, 61, 62]

As soon as the addition of PmPD-Cu nanoparticles into the As(V) solution, abundant As(V) was adsorbed by $=N^+$– components via electrostatic attraction. Meanwhile, the redox reaction between part of As(V) and nearby imine group (–NH–) occurred which produced the =N– and As(III). Therein, As(III) can readily tend to interacts with =N– through coordination.

Conclusions

In this study, a sustainable synthesis approach of Cu-loaded PmPD particles with hollow morphologies was successfully proposed based on Cu-catalysed air oxidation. The maximal conversion rate is nearly 100%, much higher than other previous reports. The TOC in filtrate is less than 10 mg L^{-1} and can be directly re-used for air oxidation to eliminate secondary pollution. This work clearly indicates the importance of Cu in the air oxidation to prepare PmPD particles by facilitating the electron transfer from ligand to O_2. In addition, the increase of Cu/mPD ratio tends to definitely constitute hollow morphology of PmPD particles. The explanation can be attributed to dehydration effect, which is beneficial for forming more stable and enlarged amphiphilic aggregates and finally form the hollow nanosized particles. Moreover, the Cu loaded PmPD particles show ability toward As(V) removal in aqueous solution with a maximal adsorbance of 27.4 mg g^{-1}. The adsorption behaviour can be well described by Freundlich and pseudo-second-order model. Altogether, by using air as a costless green oxidant, the presented idea provides a significant green strategy for high efficiency and mass production of PmPD particles. The obtained Cu-loaded PmPD particles is a promising adsorbent for As removal in environmental protection and is potentially capable of being used in many fields, as a new composite materials, such as biosensors, catalysis and anticorrosion, etc.

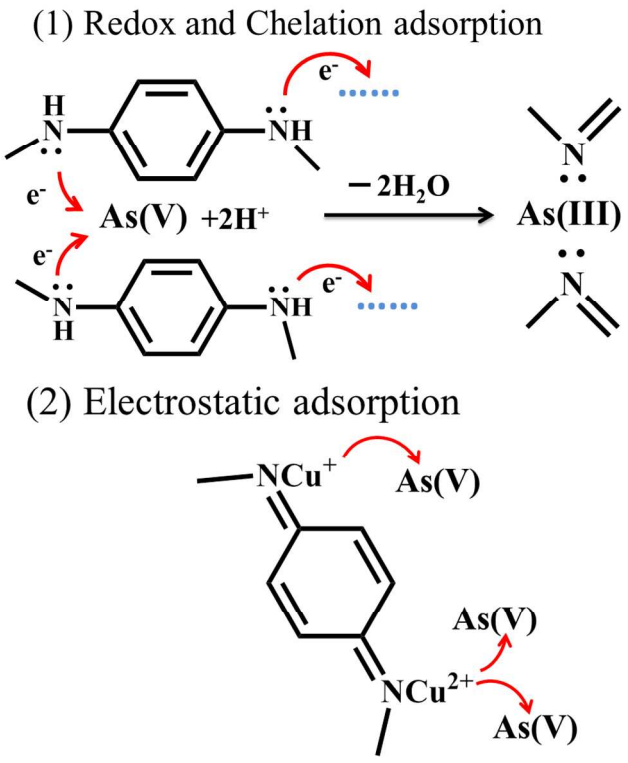

Scheme 1 Possible mechanism for arsenic adsorption with PmPD particles.

Acknowledgements

This work was supported by National Natural Science Foundation of China（51304251, 51374237）; Special Program on Environmental Protection for Public Welfare

(201509050); Shanghai Tongji Gao Tingyao Environmental Science & Technology Development Foundation and Young Scholarship Award for Doctoral Candidate Issued by Ministry of Education (1343-76140000018).

Notes and references

[a] School of Metallurgy and Environment, Central South University, Changsha 410071, China.
[b] National Research Centre for Heavy Metal Pollution Prevention & Control, Changsha 410017, China.
[c] School of Civil and Environmental Engineering, Georgia Institute of Technology, Atlanta, GA 30332-0355, United States
[d] The authors declare no competing financial interest. Shuo Dai, Bing Peng and Liyuan Zhang contributed equally to this work.

† Electronic Supplementary Information (ESI) available: [ESI-1 Equipment; ESI-2 Synthesis sketch map; ESI-3 Conversion rate of monomer, Total TOC and Cu in filtrate of PmPD particles; ESI-4 SEM and TEM images of PmPD-Cu*1:1* in different time; ESI-5 Raman spectra of PmPD particles; ESI-6 Parameters of Langmuir and Freundlich models simulated by no-liner fit for the adsorption of arsenic on PmPD particles; ESI-7 Kinetic parameters of Pseudo-first and - models for the adsorption of arsenic on PmPD-Cu*1:0.25*; ESI-8 Effect of coexisting ions on AsO_4^{3-} adsorption with PmPD-Cu*1:0.25*]. See DOI: 10.1039/b000000x/

1. Q. F. Lü, M. R. Huang and X. G. Li, *Chem.-Eur. J.*, 2007, **13**, 6009-6018.
2. M. R. Huang, Y. B. Ding and X. G. Li, *Analyst*, 2013, **138**, 3820-3829.
3. M. R. Huang, X. W. Rao, X. G. Li and Y. B. Ding, *Talanta*, 2011, **85**, 1575-1584.
4. J. Huang, S. Li, M. Ge, L. Wang, T. Xing, X. Liu, G. Chen, S. S. Al-Theyab, K.-Q. Zhang, T. Chen and Y. Lai, *J. Mater. Chem. A*, 2014.
5. M. R. Huang, H. J. Lu and X. G. Li, *J. Colloid Interface Sci.*, 2007, **313**, 72-79.
6. F. Lü, X. Feng, L. Liu and S. Wang, *Chin. Sci. Bull.*, 2013, **58**, 4039-4044.
7. X. G. Li, W. Duan, M. R. Huang and L. N. J. Rodriguez, *Reactive and Functional Polymers*, 2005, **62**, 261-270.
8. X. G. Li, W. Duan, M. R. Huang, Y. L. Yang, D. Y. Zhao and Q. Z. Dong, *Polymer*, 2003, **44**, 5579-5595.
9. X. G. Li, X. L. Ma, J. Sun and M. R. Huang, *Langmuir*, 2009, **25**, 1675-1684.
10. J. J. Wang, J. Jiang, B. Hu and S. H. Yu, *Adv. Funct. Mater.*, 2008, **18**, 1105-1111.
11. M. R. Huang, H. J. Lu, W. D. Song and X. G. Li, *Soft Materials*, 2010, **8**, 149-163.
12. L. Zhang, T. Wang, H. Wang, Y. Meng, W. Yu and L. Chai, *Chem. Commun. (Camb.)*, 2013, **49**, 9974-9976.
13. W. Yu, L. Chai, L. Zhang and H. Wang, *Trans. Nonferrous Met. Soc. China*, 2013, **23**, 3490-3498.
14. L. Zhou, Y. Wang, Z. Liu and Q. Huang, *J. Hazard. Mater.*, 2009, **161**, 995-1002.
15. Z. Su, L. Zhang, L. Chai, H. Wang, W. Yu, T. Wang and J. Yang, *New J. Chem.*, 2014.
16. X. G. Li, R. Liu and M. R. Huang, *Chem. Mater.*, 2005, **17**, 5411-5419.
17. L. Zhang, H. Wang, W. Yu, Z. Su, L. Chai, J. Li and Y. Shi, *J. Mater. Chem.*, 2012, **22**, 18244.
18. M. R. Huang, H. J. Lu and X. G. Li, *J. Mater. Chem.*, 2012, **22**, 17685-17699.
19. Z. Chen, C. Della Pina, E. Falletta and M. Rossi, *J. Catal.*, 2009, **267**, 93-96.
20. L. Zhang, L. Chai, H. Wang and Z. Yang, *Mater. Lett.*, 2010, **64**, 1193-1196.
21. Y. Wang, X. Jing and J. Kong, *Synth. Met.*, 2007, **157**, 269-275.
22. N. Bicak and B. Karagoz, *J. Polym. Sci. [A1]*, 2006, **44**, 6025-6031.
23. Z. Sun, Y. Geng, J. Li, X. Jing and F. Wang, *Synth. Met.*, 1997, **84**, 99-100.
24. W. Yu, L. Zhang, Y. Meng, S. Dai, Z. Su, L. Chai and H. Wang, *Synth. Met.*, 2013, **176**, 78-85.
25. S. Bourdo, B. Berry and T. Viswanathan, *J. Appl. Polym. Sci.*, 2005, **98**, 29-33.
26. X. G. Li, W. Duan, M. R. Huang and Y. Yang, *J. Polym. Sci. [A1]*, 2001, **39**, 3989-4000.
27. D. J. Pezolt, S. J. Collick, H. A. Johnson and L. A. Robbins, *Environ. Prog.*, 1997, **16**, 16-19.
28. M. L. Chen and Z. H. Zhou, *Polyhedron*, 2014.
29. R. Procaccini, W. Schreiner, M. Vázquez and S. Ceré, *Appl. Surf. Sci.*, 2013, **268**, 171-178.
30. L. Chai, T. Wang, L. Zhang, H. Wang, W. Yang, S. Dai, Y. Meng and X. Li, *Carbon*, 2014.
31. H. Wang, L. Chai, A. Hu, C. Lü and B. Li, *Polymer*, 2009, **50**, 2976-2980.
32. J. K. Harris, G. D. Rose and M. L. Bruening, *Langmuir*, 2002, **18**, 5337-5342.
33. H. Li, Y. Lai, J. Huang, Y. Tang, L. Yang, Z. Chen, K. Zhang, X. Wang and L. P. Tan, *J. Mater. Chem. B*, 2014.
34. J. Dey, S. Kumar, S. Nath, R. Ganguly, V. Aswal and K. Ismail, *J. Colloid Interface Sci.*, 2014, **415**, 95-102.
35. P. Sang, Y. Wang, L. Zhang, L. Chai and H. Wang, *Trans. Nonferrous Met. Soc. China*, 2013, **23**, 243-252.
36. X. G. Li, L. X. Wang, Y. Jin, Z. L. Zhu and Y. L. Yang, *J. Appl. Polym. Sci.*, 2001, **82**, 510-518.
37. L. Chai, L. Zhang, H. Wang, W. Yu and P. Sang, *Mater. Lett.*, 2010, **64**, 2302-2305.
38. X. G. Li, M. R. Huang, W. Duan and Y. L. Yang, *Chem. Rev.*, 2002, **102**, 2925-3030.
39. M. Liu, M. Ye, Q. Yang, Y. Zhang, Q. Xie and S. Yao, *Electrochim. Acta*, 2006, **52**, 342-352.
40. G. Ćirić-Marjanović, B. Marjanović, P. Bober, Z. Rozlívková, J. Stejskal, M. Trchová and J. Prokeš, *Journal of Polymer Science Part A: Polymer Chemistry*, 2011, **49**, 3387-3403.
41. M. Huang, X. Li and Y. Yang, *Polym. Degrad. Stab.*, 2000, **71**, 31-38.
42. G. Ćirić-Marjanović, M. Trchová and J. Stejskal, *J. Raman Spectrosc.*, 2008, **39**, 1375-1387.
43. W. T. Yu, L. Y. Zhang, H. Y. Wang and L. Y. Chai, *J. Hazard. Mater.*, 2013, **260**, 789-795.
44. L. Zhang, L. Chai, J. Liu, H. Wang, W. Yu and P. Sang, *Langmuir*, 2011, **27**, 13729-13738.
45. I. Losito, C. Malitesta, I. De Bari and C.-D. Calvano, *Thin Solid Films*, 2005, **473**, 104-113.
46. J. M. Lázaro Martínez, E. Rodríguez-Castellón, R. M. T. Sánchez, L. R. Denaday, G. Y. Buldain and V. Campo Dall'Orto, *J. Mol. Catal. A: Chem.*, 2011, **339**, 43-51.
47. R. L. Frost, Y. Xi and B. J. Wood, *Thermochim. Acta*, 2012, **545**, 157-162.
48. B. Pelissier, A. Beaurain, H. Fontaine, A. Danel and O. Joubert, *Microelectron. Eng.*, 2009, **86**, 1013-1016.
49. R. S. Vieira, M. L. M. Oliveira, E. Guibal, E. Rodríguez Castellón and M. M. Beppu, *Colloids Surf., A*, 2011, **374**, 108-114.
50. M. R. Huang, Q. Y. Peng and X. G. Li, *Chem.-Eur. J.*, 2006, **12**, 4341-4350.
51. L. Zhirong, A. Uddin and S. Zhanxue, *Spectrochim. Acta, Part A*, 2011, **79**, 1013-1016.
52. M. H. Habibi and B. Karimi, *J. Ind. Eng. Chem.*, 2014, **20**, 1566-1570.
53. C. Sheindorf, M. Rebhun and M. Sheintuch, *J. Colloid Interface Sci.*, 1981, **79**, 136-142.
54. T. Wang, L. Zhang, H. Wang, W. Yang, Y. Fu, W. Zhou, W. Yu, K. Xiang, Z. Su, S. Dai and L. Chai, *ACS Appl. Mater. Interfaces*, 2013, **5**, 12449-12459.
55. S. Saha and P. Sarkar, *J. Hazard. Mater.*, 2012, **227–228**, 68-78.

56. T. D. Çiftçi and E. Henden, *Powder Technol.*, 2015, **269**, 470-480.
57. L. Yan, H. Yin, S. Zhang, F. Leng, W. Nan and H. Li, *J. Hazard. Mater.*, 2010, **178**, 209-217.
58. M. Ayad, W. Amer and J. Stejskal, *Thin Solid Films*, 2009, **517**, 5969-5973.
59. J. Han, J. Dai and R. Guo, *J. Colloid Interface Sci.*, 2011, **356**, 749-756.
60. J. Stejskal, M. Trchová, L. Brožová and J. Prokeš, *Chem. Pap.*, 2009, **63**, 77-83.
61. C. Izumi, H. F. Brito, A. M. D. Ferreira, V. R. Constantino and M. L. Temperini, *Synth. Met.*, 2009, **159**, 377-384.
62. M. R. Huang, S. J. Huang and X. G. Li, *The Journal of Physical Chemistry C*, 2011, **115**, 5301-5315.

